Acta metall. Vol. 31, No. 11, pp. 1849–1860, 1983
Printed in Great Britain.

0001-6160/83/ $3.00 + 0.00

THE INTERPRETATION OF STRUCTURE FUNCTIONS IN QUENCHED BINARY ALLOYS

P. FRATZL[1], J. L. LEBOWITZ[2], J. MARRO[3] and M. H. KALOS[4]

[1]Institut für Experimentalphysik der Universität Wien, Strudlhofgasse 4, 1090 Wien, Austria, [2]Department of Mathematics and Physics, Rutgers University, Busch Campus, New Brunswick, NJ 08903, U.S.A., [3]Departemento de Física Teórica y Departemento de Ecuationes Funcionales, Universidad de Barcelona, Diagonal 647, Barcelona 28, Spain and [4]Courant Institute of Mathematical Sciences, New York University, New York, NY 10012, U.S.A.

(*Received* 5 *March* 1983; *in revised form* 26 *May* 1983)

Abstract—We study the segregation process in quenched binary alloys by analyzing and comparing the time evolution of the structure function and of the grain distribution obtained from computer simulations on a model system. We find good agreement between cluster sizes and densities determined directly on the computer sample and ones obtained by the Guinier method from the structure function. We then describe a graphical method for determining the scaling behaviour of the structure function $S(k, t)$ which gives good statistics because the whole curve $S(k, t)$ vs k is used. This yields very good agreement between the scaling function (scaled with the Guinier radius) obtained from the computer simulations and from a variety of real experiments. This function shows a universal behaviour independent of the alloy composition, the temperature and even the substance investigated. Our results are also not consistent with the more recent theoretical work (Binder *et al.*, Furukawa *et al.*) which give alternate derivations and extensions of the Guinier formulas.

Résumé—Nous avons étudié la décomposition d'alliages binaires après trempe par une analyse comparée de l'évolution en temps de la fonction de structure et de la distribution des grains de précipité, obtenues par simulation sur ordinateur à l'aide d'un modèle d'Ising. Il y a bon accord entre la taille et la densité des précipités déterminées d'une part directement sur l'échantillon Ising et d'autre part suivant la méthode de Guinier à partir de la fonction de structure. Ensuite nous décrivons une méthode graphique permettant de déterminer la loi d'échelle concernant la fonction de structure $S(k, t)$ avec une bonne statistique puisque toute la courbe $S(k, t)$ vers k est utilisée. La fonction obtenue en réduisant les échelles avec le rayon de Guinier, autant pour les simulations que pour différents systèmes réels, s'avère universelle indépendamment de la composition de l'alliage, de la température et même de la nature de l'échantillon. Nous résultats ne sont pas en accord même avec les travaux théoriques plus récents (Binder *et al.*, Furukawa *et al.*) qui redémontrent et généralisent les formules de Guinier.

Zusammenfassung—Der isotherme Entmischungsprozess in binären Legierungen wird mit Computersimulationen an einem Modellsystem untersucht, indem die zeitliche Veränderung der Strukturfunktion sowie die Verteilung der Ausscheidungsteilchen analysiert und verglichen werden. Teilchengröße- und Anzahl, bestimmt einerseits durch direktes Abzählen an der Probe und andererseits durch Anwenden der Guiniermethode an die Strukturfunktion, stimmen gut überein. Weiters wird eine graphische Methode zur Bestimmung des Skalierungsverhaltens beschrieben, die eine große Genauigkeit erlaubt, weil die gesamt Kurve $S(k, t)$ gegen k verwendet wird. Man erreicht dadurch eine sehr gute Übereinstimmung zwischen allen Skalierungsfunktionen [$S(k, t)$ skaliert mit dem Guinierradius], die für die Computersimulationen sowie eine Reihe von realen Systemen bestimmt wurden. Es wird daher auf eine universelle Funktion geschlossen, die unabhängig ist von dem Mischungsverhältnis in der Legierung, der Temperatur und sogar der untersuchten Substanz. Unsere Ergebnisse sind auch mit neueren theoretischen Arbeiten (Binder *et al.*, Furukawa *et al.*) nicht konsistent, die neue Ableitungen und Erweiterungen der Guinier' schen Formeln angeben.

1. INTRODUCTION

Many alloys such as AlZn, which are homogeneous at high temperature, segregate when quenched into the miscibility gap. That is they form localized regions having compositions corresponding to macroscopically different phases. Physical properties of the alloy, such as hardness and resistivity, are strongly influenced by the character of the inhomogeneity, which, in turn, is determined by the kinetics of the segregation process. For this reason, the formation of structure after quenching has been extensively studied in many alloys. Quantities of particular interest include the size and composition of the grains, i.e. regions rich in one of the components precipitating out of the uniform background.

The grains can be observed in some cases directly by using electron [1] or field ion microscopy [2] or by indirect methods like resistivity [3], calorimetry [4] and EXAFS [5]. There are various limitations and drawbacks to the above techniques and a frequently used method for studying the time evolution of the

structure of quenched alloys is the small angle scattering of X-rays [6, 7], light [8] or neutrons [9–11]. This measures directly the structure function $S(k, t)$, the Fourier transform of the composition correlation function of the alloy, at any given time t after the quench. The function $S(k, t)$ contains much useful information about the density of different size grains and their spatial distribution at the time t. How to get this information deciphered is, however, by no means obvious and is the subject of our work, as it has been of many earlier studies [12–21].

It is clear from the beginning that one can define a variety of characteristic wave vectors such as $k_{max}(t)$, $k_1(t)$, corresponding to the location of the maximum of $S(k, t)$ or to the value of its first moment at time t. These will, by necessity, be related in some way to characteristic lengths of the system at time t, e.g. the "radius" of the average grain size, the composition wavelength, etc. [12–21]. What is not clear however is how to go beyond these very qualitative statements. Doing this requires some quantitative understanding of the relation between the shape of $S(k, t)$ as a function of k and the morphology of the system at time t.

It should be noted however, that, even in principle, $S(k, t)$ cannot give full information about the geometrical structure of the system; it simply doesn't contain it. What is being considered here is rather how to extract maximum information from $S(k, t)$ about the evolution of the segregation process in the system. In this connection it is important to realize that experimentally $S(k, t)$ is often known only over a limited range of k values and sometimes with rather large errors due to the high background in scattering experiments at very low k. A theoretical understanding of the structure function is therefore very important for its optimal practical utilization.

A frequently used method for analyzing experimentally obtained structure functions is due to Guinier [16]. A plot is made of ln $[S(k,t)]$ vs k^2 and the "slope" of a straight portion of this plot is used to define a mean "radius of gyration" of the clusters. The method is based on various assumptions, i.e. independent clusters, small k expansion, but is often used outside the domain of validity of such approximations; the characteristic straight lines appear in such plots even in cases, where the basic hypotheses of the model are not satisfied. It therefore seems of interest to clarify the meaning of the "radius" obtained by this method, regardless of the validity of the Guinier model, by comparing it to cluster sizes used in statistical theories. This comparison may be carried out using computer simulations, where both structure function and cluster distribution are known. These kind of simulations have been shown to give results similar to those of real experiments [15]. It was in fact these computer simulations which first showed clearly the scaling of $S(k, t)$ during the later stages of the decomposition, i.e. for late times $S(k, t)$ depends to a good approximation only on one variable $k/k_1(t)$, so it defines only one independent length scale. This was subsequently found to hold also in many experimental situations [7–9, 15]. This behaviour is also predicted or incorporated in different theoretical models [18–21] of the time evolution following quenching.

In this note the simulations of Ref. [15] plus some new ones in order to compare directly the structure function and the cluster analysis data are reanalysed. We find that there is a good agreement between the Guinier radius R_G and the mean cluster size determined directly. R_G is identified as a good scaling length of the system and therefore R_G has some physical meaning even in cases where the Guinier hypotheses are not satisfied. We also describe a direct method for deciding if experimental or computer data show a scaling behaviour and how to determine the scaling function F_G graphically. F_G is defined via the relation

$$S(k, t) = J_G(t) \cdot F_G[k \cdot R_G(t)] \tag{1.1}$$

where $R_G(t)$ and $J_G(t)$ are the scaling lengths (of the k and the S axes) determined by the Guinier method. By doing this we found in our simulation data as well as in recent experimental results on real systems, that for large x, $F_G(x)(x = k \cdot R_G)$ is independent of temperature T, density ρ, and even the substance investigated. In fact $F_G(x)$ may be written in all cases as

$$F_G(x) = \Phi(x) \cdot \Psi[x \cdot \delta(\rho, T)] \tag{1.2}$$

where Φ and Ψ are universal functions. Φ may be interpreted as describing the intensity diffracted by a single cluster and Ψ is a "cluster interference function" which differs from 1 only at small values of k, δ is a time independent constant which characterises the point in the phase diagram where the experiment is performed. It would certainly be interesting to test this "universality" in more experimental cases. It would also be very useful to find simple theoretical expressions for Φ and Ψ.

Note here that the work of Binder *et al.* [18], Furukawa [19], Rikvold and Gunton [20] and Ohta *et al.* [21] provides a more general framework for discussing the scaling of the structure function and *ipso facto* the scaling length R which enters there, than does the original work of Guinier [16]. We have couched most of our discussion in the language of Guinier. Because (a) it is the seminal work on the subject and in fact leads to essentially the same final formulae as do the more recent works, compare for example equations (59) and (66) in [16] with equations (1) and (2) in [20] and (b) it provides a simple picture of the segration process and gives concrete prescriptions for finding $R_G(t)$ which are universally used by metallurgists. Even when the Guinier picture is not literally applicable it provides useful qualitative insights into a very complex process. Our analysis here is intended to extend the Guinier picture without losing its simplicity. This will hopefully provide the metallurgist with practically useful methods for analyzing experiments. It also provides new quantitative data on which future more complete theories, which combine the Guinier picture with the more general scaling analyses, can be based.

2. MODELS AND APPROXIMATIONS

2.1. Simulations

The model system is described in detail elsewhere [15]. It is a simple cubic lattice with $N = L^3$ ($L = 30$ or 50 in the present simulations) lattice sites each occupied by either an A or B atom. We use periodic boundary conditions. The number of A-atoms is given by ρN, ρ being their density. Starting with a random distribution of the A and B atoms on the lattice (corresponding to equilibrium at very high temperatures), the system is quenched into the miscibility gap at a given temperature. The evolution of the system is governed by Kawasaki dynamics [22] with nearest neighbor exchanges. The exchange probability of neighboring A and B atoms is given by

$$P = \exp(-\beta \cdot \Delta U) \cdot [1 + \exp(-\beta \cdot \Delta U)]^{-1} \quad (2.1)$$

where $\beta = 1/k_B T$ (k_B is the Boltzmann constant) and ΔU is the change in the energy

$$U = -J \sum_{nn} \eta(\mathbf{r}_i) \cdot \eta(\mathbf{r}_j);\ J > 0 \quad (2.2)$$

due to the exchange. The sum in (2.2) is over nearest neighbor pairs; $\eta(\mathbf{r}_i)$ is $1(-1)$ if there is an A(B) atom at site $\mathbf{r}_i$. Each nearest neighbor pair is chosen at a rate $\alpha/3$ and an exchange is accepted with probability $P \cdot \alpha^{-1}$ is then the average time between two attempts to change the occupation of a given lattice site and we take it as our time unit. The miscibility gap for this model is represented in Fig. 1: the critical temperature is $T_c = 4\,\mathrm{J}/0.88686\,k_B$ [23]. The points where simulations were performed are indicated in Fig. 1 and described in Table 1.

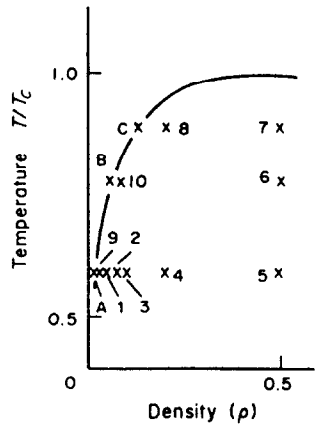

Fig. 1. Phase diagram of the binary Ising model. The crosses indicate points where computer experiments have been performed. Points A, B and C are on the coexistence line; points 9 and 10 are inside the miscibility gap but appeared to be metastable states; at points 1–8 the decomposition process has been observed. A more precise description of these points is given in Table 1.

2.2. Cluster analysis

Clusters are defined in the computer simulations as groups of A-atoms connected by nearest neighbor bonds. A cluster containing j A-atoms is called a j-cluster. We call the number of j-clusters in the sample $n(j)$, so that

$$\sum_j j \cdot n(j) = \rho N. \quad (2.3)$$

This definition is useful only for $\rho \lesssim 0.2$ when the clusters of A-atoms may be identified with the grains of the minority phase. The development of large clusters following quenching then corresponds to coarsening of the alloy. For $\rho > 0.20$ the system soon develops clusters of infinite size, even on the coexistence line [15]. It was found in the computer simulations at low

Table 1. Description of all points in the ising model phase diagram (Fig. 1) where computer experiments were performed

Point in Fig. 1	Temperature (T/T_c)	Density (ρ)	No. of averaged independent runs	Lattice size (L)	Max. duration of run	Min. time of scaling
1	0.591	0.050	1	50	14,000	8000
2	0.591	0.075	1	50	10,200	5000
3	0.591	0.100	1	50	7300	3000
4	0.591	0.200	8	30	3900	900
5	0.591	0.500	8	30	3600	300
6	0.780	0.500	8	30	1700	700
7	0.887	0.500	8	30	6600	500
8	0.887	0.200	8	30	1700	400
9	0.591	0.035	1	50	16,000	Metastable state
10	0.780	0.075	1	50	800	Metastable state
A	0.591	0.01456	1	50	Equilibrium at coexistence line	
B	0.780	0.06130	1	50	Equilibrium at coexistence line	
C	0.887	0.12463	1	50	Equilibrium at coexistence line	

Points A, B and C are equilibrium states at the coexistence line and the equilibrium structure functions were used for background determination (see Section 2.3). Points 9 and 10 were metastable states inside the miscibility gap, whereas at points 1–8 decomposition occurred. The maximum duration of each run and the time needed to reach scaling behaviour are indicated in units of α^{-1} (see Section 2.1). The size of the lattice was 50 × 50 × 50 or 30 × 30 × 30. In the latter case 8 independent runs have been averaged to get better statistics.

densities [15] that, after some initial time, $n(j)$ varies slowly with time for $j < 10$. For comparison with experimental data we define an average cluster size by

$$j_1 = \sum_{j>j_c} j \cdot n(j) \Big/ \sum_{j>j_c} n(j) \tag{2.4}$$

where j_c is an arbitrary cutoff. For the present analysis we have taken cutoffs of 10, 20 and 50. We also define

$$n_1 = \sum_{j>j_c} n(j) \tag{2.5}$$

the number of clusters greater than j_c. Thus

$$N_1 = j_1 \cdot n_1 \tag{2.6}$$

is the number of A-atoms in clusters bigger than j_c.

2.3. *Structure function*

The intensity scattered in a neutron or X-ray small-angle scattering experiment $I(\mathbf{k}, t)$ may be related to the model structure function $J(\mathbf{k}, t)$ calculated in the computer simulation on a lattice of size $N = L^3$ by

$$\frac{I(\mathbf{k}, t)}{I_0 \cdot N} = J(\mathbf{k}, t) = N^{-1}\left\langle \left| \sum_j \exp(i\mathbf{k}\cdot\mathbf{r}_j)\cdot\sigma(\mathbf{r}_j, t)\right|^2 \right\rangle \tag{2.7}$$

where σ indicates the site occupation [24], it is 1 if there is an A-atom at the lattice site $\mathbf{r}_j$ and 0 otherwise. $\mathbf{I}_0$ is a constant (for X-rays I_0 is slightly k-dependent [16]) depending essentially on the scattering lengths of the A and B atoms.

We define the function

$$S(\mathbf{k}, t) = J(\mathbf{k}, t) - J_{eq}(\mathbf{k}) \tag{2.8}$$

where J_{eq} is the equilibrium intensity (computed like J) at the coexistence line at the same temperature as J. This background subtraction has been discussed in detail in Ref. [15]. In most experiments on real systems this background is not available and therefore a constant background (Laue level) or no background at all is subtracted. In the simulations too, after some initial time, and at temperatures not too close to T_c (so that the fluctuations and therefore J_{eq} are small) J_{eq} is small compared to $J(\mathbf{k}, t)$ and may be neglected. At the very early times of the decomposition however J and J_{eq} may be of the same size and one has to be very careful in the interpretation of the structure function.

To simulate an experiment on a polycrystal we have performed a spherical average of $S(\mathbf{k}, t)$ and the structure function so obtained is finally written $S(k, t)$. The present definition is slightly different from that in Ref. [15] but is more consistent with the notations used in classical small-angle scattering theories [16]. It is related to the function S_1 defined in Ref. [15] by a simple formula

$$S(k, t) = \frac{1}{4}(m_0^2 - \bar{\eta}^2)\, S_1(k, t) \tag{2.9}$$

where $\bar{\eta} = 1 - 2p$ and m_0 is the value of $\bar{\eta}$ at the co-existence density. For details see Ref. [15].

3. GUINIER ANALYSIS OF THE STRUCTURE FUNCTION

At low densities of A-atoms the A-rich and A-poor regions are expected to be separated by sharp interfaces. When one assumes widely separated identical clusters (so that there is no interference between them) the Guinier approximations should be valid and the scattered intensity will take a Gaussian shape for small values of k, i.e.

$$S(k, t) \approx J_G(t) \cdot \exp\left(-\frac{R_G^2(t)}{5} k^2\right) \tag{3.1}$$

$R_G(t)$ is then identified as $\sqrt{5/3}$ times the radius of gyration of the cluster, (for a spherical cluster R_G would be its radius) while $J_G(t)/R_G^6(t)$ should be proportional to the number of clusters in the sample. Comparing this with the definitions (2.4–2.6) one would expect, when (3.1) is valid, that

$$j_1 \propto V_G = \frac{4}{3}\pi R_G^3 \tag{3.2}$$

$$N_1 \propto J_G/V_G. \tag{3.3}$$

Generally R_G and J_G in (3.1) are determined by fitting a straight line to the curve $\ln [S(k, t)]$ against k^2. It is found however that for very low k (which corresponds to long distance correlations) there is a deviation from the Gaussian shape. This is taken into account [16] by writing

$$S(k, t) = J_G(t) \cdot \exp\left(-\frac{R_G^2(t)}{5} k^2\right) \cdot H(k, t) \tag{3.4}$$

where $H(k, t)$ is equal to 1 for large k. The straight line used for finding R_G and J_G thus appears only in a portion of the curve $S(k, t)$ against k^2: a portion which is often outside the domain of validity of the hypotheses which Guinier made to derive his model. This is the case, in fact, for our computer simulations. Such a plot with its straight portion may be seen in Fig. 7 (although the scales are reduced there, as explained later on in the paper). Since the Guinier method is nevertheless used quite successfully in practice it is particularly interesting. It should also be mentioned here that the Gaussian shape is not expected to hold for very large k. An estimation first carried out by Porod [16] predicts an asymptotic behaviour like k^{-4} of the structure function.

3.1. *Test of the Guinier method for low densities*

In the case of low densities ρ, cluster sizes obtained by the Guinier method from the structure function can be compared to those obtained by direct observation of the sample. The information one expects to get from the Guinier plot is the mean volume of the clusters $V_G = 4/3\pi R_G^3$ (3.2), and the total number of A-atoms in large clusters, which is proportional to J_G/V_G (3.3).

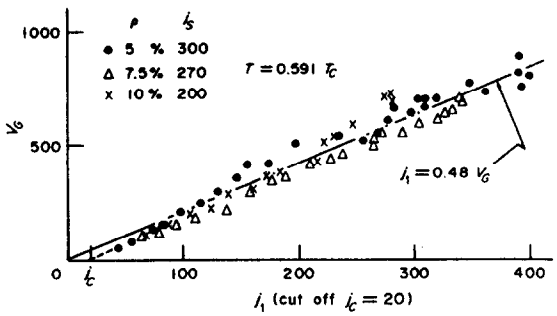

Fig. 2 The volume of the mean cluster determined by the Guinier method V_G is plotted vs the mean cluster size l_1 determined directly with $l_c = 20$ (see Section 2.2) for three different densities at $T = 0.591\ T_c$. l_1 is growing with time, so that the minimum size l_s, corresponding to the minimum time where the structure function scales, may be determined. The values of l_s are indicated in the figure.

In Figs 2 and 3, V_G and J_G/V_G obtained from fits of ln S vs k^2 have been plotted against j_1 and N_1, which were computed with various cutoffs j_c (see Section 2.2), for the densities 5, 7.5 and 10%.

There is a good linear relation between V_G and j_1 for $j_c = 20$ (Fig. 2). j_1 computed for $j_c = 10$ or 50 gave a similar behaviour but more scattering of the data points. The relation

$$j_1 \approx \frac{1}{2} V_G \tag{3.5}$$

holds for times much earlier than the beginning of the scaling regime. j_1 is growing with time and one may determine its value at the time when the structure function begins to scale. This value is denoted by j_s and is indicated in Fig. 2 where one may see that relation (3.5) holds for j_1 much smaller than j_s. Only at very early times is there a small deviation from this relation, because j_1 is sensitive to the cutoff (j_1 is always larger than j_s).

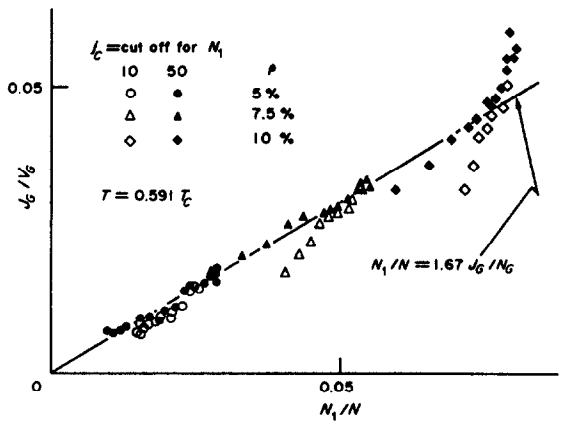

Fig. 3. The total volume of A-atoms in the large clusters determined by the Guinier method J_G/V_G is plotted against the number N_1 of A-atoms in clusters greater than 10 (open symbols) and clusters greater than 50 (solid symbols) determined directly (see Section 2.2). Three different densities at $T = 0.591\ T_c$ are included and there is a fairly good linear dependence for $l_c = 50$.

In Fig. 3 it can be seen that, when a cutoff of 50 is used for N_1, the relation

$$N_1/N \approx \frac{5}{3} J_G/V_G \tag{3.6}$$

holds for all three densities (5, 7.5 and 10%) and all times except for very late times of the run at $\rho = 10\%$. Nevertheless this direct proportionality between N_1 and J_G/V_G is very sensitive to the choice of the cutoff used for the computation of N_1. For $j_c = 10$ and 20 the dependence (3.6) does not hold any more (see Fig. 3 for the case $j_c = 10$). The fact that J_G/V_G is more consistent with N_1 computed with a cutoff at 50 than at 10, seems reasonable because the Guinier approximation which uses a radius of gyration, gives more weight to the bigger clusters. It appears therefore from Figs 2 and 3 that if the right cutoff for j_1 and N_1 is chosen, a good agreement between V_G and j_1 on one hand and J_G/V_G and N_1 on the other may be obtained. The agreement in both cases then holds for times much earlier than the beginning of the scaling regime. Hence one can expect good results from the Guinier method even before the scaling regime.

The cluster sizes and densities so obtained seem to be more satisfactory representations of the complicated microscopic structure of the involving system than the ones obtained with k_1 in Ref. [15]. The slope of k_1 vs j_1 depends on the density whereas the slope of V_G vs j_1 is the same for $\rho = 5$, 7.5 and 10%.

3.2. *Integrated intensity*

Another classical method to evaluate N_1, the total number of atoms in large clusters is via the so called "integrated intensity" $\bar{S}(t)$, the integral of $S(\mathbf{k}, t)$, where $|\mathbf{k}|$ varies between 0 and a given cutoff $\mathcal{K}$ defined in practice by the experimental conditions

$$\bar{S}(t) = N^{-1} \sum_{|\mathbf{k}| \leq \mathcal{K}} S(\mathbf{k}, t) \tag{3.7}$$

(for the simulations we took $\mathcal{K} = 0.55\pi$. At low densities a linear dependence between $\bar{S}$ and N_1 may be expected [16]. In Fig. 4, $\bar{S}$ has been plotted vs N_1 for ρ

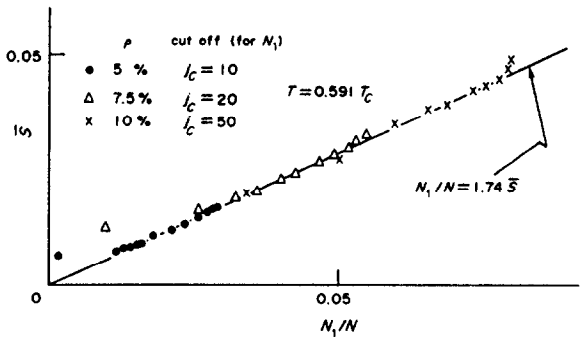

Fig. 4. The integrated intensity $\bar{S}$ is plotted against the total number N_1 of A-atoms in clusters greater than l_c. Three densities at $T = 0.591\ T_c$ are included and different cutoffs l_c had to be taken for each density to get a good linear dependence.

= 5, 7.5 and 10%. One finds a good linear dependence if one takes a different cutoff j_c of N_1 for each density ρ (see Fig. 4).

The relation between N_1 and $\bar{S}$ (Fig. 4)

$$N_1/N \approx \frac{7}{4}\bar{S}(t) \tag{3.8}$$

is very close to the one between N_1 and J_G/V_G (3.6). However, as already mentioned, to get the linear dependence (3.8) N_1 had to be computed with a cutoff dependent on the mean density ρ throughout the crystal, whereas (3.6) was obtained with the same cutoff $j_c = 50$ for each ρ. This may be due to the fact that the integrated intensity is strongly influenced by the atoms in small clusters, whereas in the Guinier method the bigger clusters predominate. (We have however, no convincing evidence for this.)

3.3. *Higher densities*

An essential hypothesis for the exponential approximation of Guinier is that the clusters are widely separated. This may be true in the case of low densities but it is certainly not so at $\rho = 50\%$ where only one cluster contains most of the A-particles. Even in this case, however, a "Guinier radius" may be determined by the usual method. Since j_1 is now approximately equal to N_1, it is no longer proportional to V_G. One must therefore find some other way to relate R_G to a characteristic length of the system. One such way is to use the energy per lattice site defined as, see equation (2.2)

$$U/N - 3 = E = E_0 N^{-1} \nu_{nn} \tag{3.9}$$

where ν_{nn} is the total number of nearest neighbor A–B bonds in the system and $E_0 = 2J$. Letting

$$E_e = 6E_0 \cdot \rho_e(1-\rho_e) \tag{3.10}$$

be the energy corresponding to either of two uniform phases $\rho_e = \rho$ at the coexistence line ($\rho_e = 1.5\%$ at $T = 0.59\, T_c$), $E - E_e$ may be interpreted as a measure of the total surface of the interface boundaries. In the case of low densities, if one assumes spherical clusters of radius r and a cluster density n, then $E - E_e$ is proportional nr^2. If the total volume of the clusters remain nearly constant, $nr^3 = \text{const.} \sim \rho - \rho_e$, then one may expect $(E-E_e)^{-1}$ to be proportional to r. In Fig. 5(a) the Guinier radius R_G has been plotted vs $(E-E_e)^{-1}$ for $T = 0.591\, T_c$ and the densities 5, 7.5, 10 and 50%. For each density the product $V = R_G(E-E_e)$ is in fact nearly constant. The ratio $V/(\rho-\rho_e)$ is not exactly constant and gives some indication of the shape of the interfacial region, greatly decreasing for 50% when there are no isolated large clusters (see Table 2). The interpretation of the Guinier radius in terms of the total surface of the interface boundaries provides a certain physical significance for R_G at higher densities which might be possible to check in real systems.

In addition the total energy E has been plotted in Fig. 5(b) against $t^{-1/3}$, where t is time in units of α^{-1}. Straight lines have been fitted to the curves, but the values for E extrapolated at infinite time do not correspond to the equilibrium value E_e, as one would expect.

4. SCALING BEHAVIOUR

It was shown in Ref. [15] that the structure function scales dynamically for late times. In the scaling regime

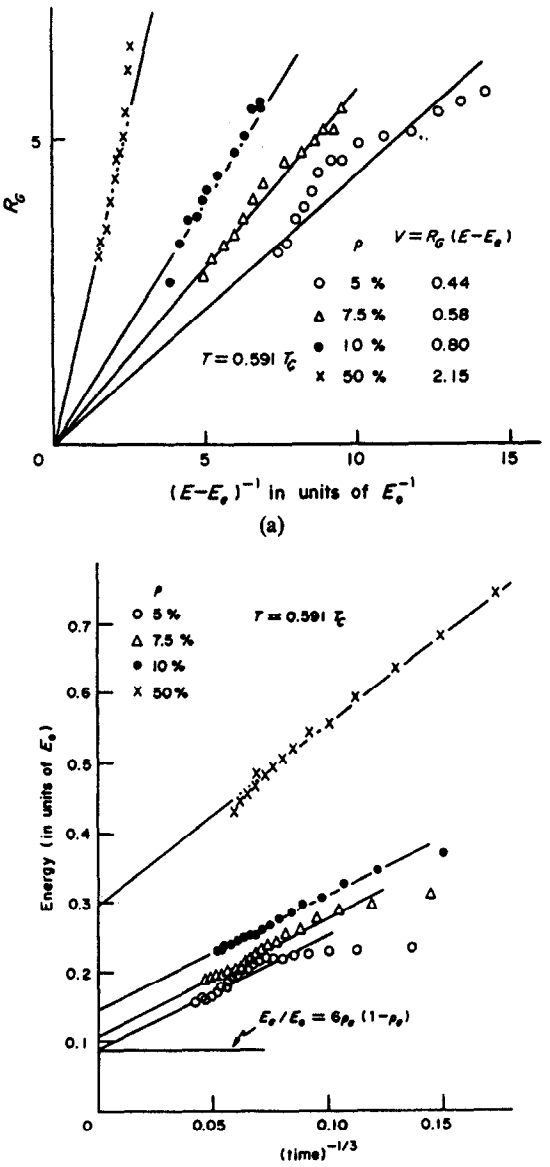

Fig. 5.(a) The Guinier radius R_G is plotted against the inverse of the total energy $(E-E_e)^{-1}$ for several densities at $T = 0.591\, T_c$. There seems to be a linear dependence in each case and the slope $V = R_G(E-E_e)$ in indicated. (b) The total energy has been plotted against $t^{-1/3}$, where t is time in units of α^{-1}, for several densities at $T = 0.591\, T_c$. Straight lines could be fitted to the curves, which might be related with a $t^{1/3}$ behaviour of R_G. Nevertheless the energy extrapolated at infinite time is different from E_e. It has been tried to use this extrapolated value instead of E_e as the bulk energy, but then the plot analogous to Fig. 5(a) did not show anymore a good linear dependence between R_G^{-1} and the energy.

Table 2. Several constants of the scaling regime

Sample	Density	Temperature (T/T_c)	δ	$k_s = k_1$ α_s	β_s	$k_s = k_m$ α_s	β_s	$V/(\rho - \rho_c)$
	0.05	0.591	0.78	1.94	1.30			12.4
	0.075	0.591	0.66	2.02	1.50			9.6
	0.10	0.591	0.40	2.35	3.00	2.30	2.93	9.4
	0.20	0.591	0.37	2.61	4.80	2.42	5.33	
Ising model	0.50	0.591	0.34	2.72	6.36	2.57	7.80	4.4
	0.50	0.780	0.37	2.66	5.00	2.42	5.85	
	0.50	0.887	0.43	2.32	2.64	1.99	2.36	
	0.20	0.887	0.54	1.85	2.08	1.68	2.22	
Au–60 at.%Pt	0.40	0.6	0.37					
$80B_2O_3$–$15PbO$–$5Al_2O_3$	(wt%)	0.77	0.38					
$64B_2O_3$–$27PbO$–$9Al_2O_3$	(wt%)	0.80	0.34					

$\alpha_s = R_G(t) \cdot k_s(t)$ and $\beta_s = J_G(t)/J_s(t)$ are constant when the structure function is scaling (see Section 4.1) and are indicated here in the case $k_s = k_1$ (first moment) and $k_s = k_m$ (position of the maximum). $V = (E - E_c) \cdot R_G$ defines the relation between Guinier radius and total energy of the system (see Section 3.3). δ is the constant introduced in Section 5.3. Notice that δ is smaller as the experiment is performed deeper inside the miscibility gap. The data concerning the real systems (see Figs 9 and 10) are taken from Refs. [7] and [10].

$S(k, t)$ is described by only one characteristic length and therefore k_1^{-1}, k_m^{-1}, R_G are proportional and any of them may be used as the scaling lengths. In Ref. [15] the length used was k_1^{-1} defined as

$$k_1(t) = \sum_{k \leq \mathcal{K}} kS(k, t) \Big/ \sum_{k \leq \mathcal{K}} S(k, t) \tag{4.1}$$

4.1. Scaling function

In order to demonstrate scaling and obtain the scaling function we proceeded as follows in Ref. [15]: we set $x = k/k_1(t)$ and defined

$$F_1(x, t) = S[xk_1(t), t]/J_1(t) \tag{4.2}$$

$$J_1(t) = \frac{2\pi}{L} k_1^{-3}(t) \sum_{k \leq \mathcal{K}} k^2 S(k, t). \tag{4.3}$$

It was then observed that for each point in the miscibility gap there was some initial time period, given in Table 1, after which $F_1(x, t) \approx F_1(x)$ independent of t. The function $F_1(x)$ depended on the region in the miscibility gap to which the quench was made, without any appearent relation between the different scaling functions.

To clarify this point we shall here choose the Guinier radius as the basic scaling length and define F_G so that $[x = kR_G(t)]$

$$F_G(x, t) = S[x/R_G(t), t]/J_G(t) \tag{4.4}$$

where $J_G(t)$ is defined by relation (3.1) in the k-region where the Guinier method may be applied (see Section 3). As can be seen from (3.1) the function F_G reduces in a suitable interval of x simply to $\exp(-x^2/5)$. The scaling regime is defined by $F_G(x, t) \approx F_G(x)$ independent of time.

To clarify the relation between F_1 and F_G we note that if $k_s^{-1}(t)$ is any scaling length and $F_s(x)$ the corresponding scaling function so that $[x = k/k_s(t)]$

$$F_s(x) = S[x \cdot k_s(t), t]/J_s(t) \tag{4.5}$$

then k_s^{-1} and $J_s(t)$ are proportional respectively to $R_G(t)$ and $J_G(t)$, and the scaling function $F_s(x)$ is related simply to $F_G(x)$ by

$$F_s(x) = \beta_s \cdot F_G(\alpha_s \cdot x) \tag{4.6}$$

$$k_s^{-1}(t) = R_G(t)/\alpha_s \tag{4.7}$$

$$J_s(t) = J_G(t)/\beta_s \tag{4.8}$$

i.e. the scaling function F_s is determined uniquely by the constants $\alpha_s = R_G(t) \cdot k_s(t)$ and $\beta_s = J_G(t)/J_s(t)$. These have been computed for the case $k_s = k_1, J_s = J_1$ given in (4.2), (4.3) and for the position and height of the maximum of $S(k, t)$, that is $k_s(t) = k_{max}(t)$; $J_s(t) = J_{max}(t) = S[k_{max}(t), t]$. k_s and β_s appear indeed to be independent of time in the scaling regime and their values are listed in Table 2.

4.2. A natural scaling length

The scaling lengths introduced until now (k_1^{-1}, k_m^{-1}, R_G) are computed from the structure function without using all the information contained in it. Thus k_1^{-1} uses integrals of S, k_m^{-1} the maximum position and R_G the fit of S to a gaussian in a given k-interval. A natural way of deciding whether there is scaling and determining immediately a scaling length using the full function $S(k, t)$ is provided by the following method:

(i) ln $S(k, t)$ is plotted vs ln k for various values of $t(t_i, i = 1, m)$,

(ii) the curves for two different times t_i and t_j may be shifted with respect to each other so that the x and y axis of both plots remain parallel,

(iii) if the curves can be superposed so that they overlap exactly, the structure function scales. If not, threre is no scaling behaviour,

(i) if the structure function scales after some time t_s, one has to choose one of the curves as reference. One might use the curve $S(k, t_m)$ at the last time investigated. Then all curves for $t_s \leq t_i \leq t_m$ should be superposed on the curve at t_m so that they overlap. The difference between the k-axis at time t_i and t_m is then exactly ln $[J_s(t_i)]$ and the distance between the ln S-axes is ln $[k_s^{-1}(t_i)]$.

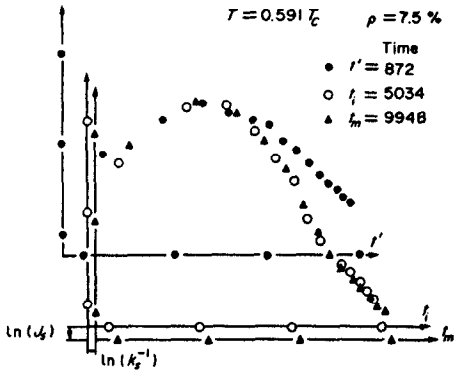

Fig. 6. The "natural scaling" method is illustrated in the case of P2 ($T = 0.591\ T_c$ and $\rho = 7.5\%$). First the structure functions $S(k, t)$ are plotted as ln S vs ln k. Then the curves at the time $t_m = 9948$ (triangles) and $t_l = 5034$ (circles) are superposed by shifting the axes so that they remain parallel. If the curve at t_m is taken as reference we have in this case ln $[k_s^{-1}(t_l)]$ and ln $[J_s^{-1}(t_l)]$ negative and given respectively by the differences of the two y-axes and the two x-axes. One may see also that at time 872 (crosses) the structure function does not yet scale.

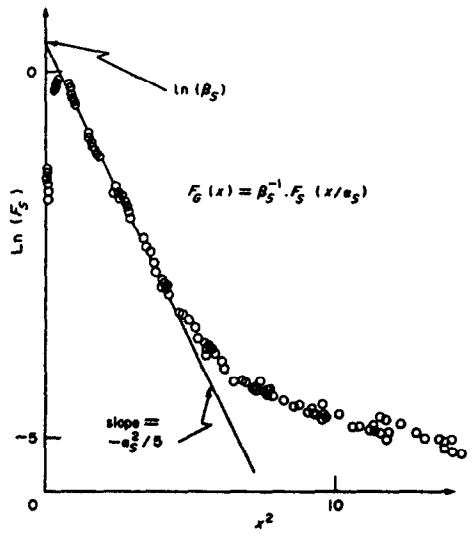

Fig. 7. Guinier plot of the scaling function F_s determined using any scaling length k_s^{-1} (see Section 4). In the case of P2 ($T = 0.591\ T_c$ and $\rho = 7.5\%$). $-\alpha_s^2/5$ is the slope of ln F_s vs x^2 and ln β_s the intercept of the straight line. The normalised scaling function F_G is then given by $F_G(x) = \beta_s^{-1} \cdot F_s(x/\alpha_s)$.

This is illustrated by Fig. 6 where some points corresponding to the simulation at point P2 (see Table 1) are plotted according to this method. $k_s^{-1}(t)$ and $J_S(t)$ are then called the natural scaling lengths. It is important to notice that no normalization of the scattered intensity or of the wave vector is necessary. Since differences in logarithmic scales are taken, all the multiplicative constants specific for each experiment drop out. Thus the wavelength of the incident beam, the lattice spacing of the sample, the detector efficiencies, the sample volume, or the diffusion lengths of the atoms in the sample have no effect on the analysis. The scaling functions, F_S, obtained by this method differ only when different times t_m are chosen for the reference scale. To get a final normalization of F_S, a Guinier plot of F_S may be performed (see Fig. 7 for the case of P2). If in a certain x-range immediately after the maximum of $F_S(x)$ a straight line appears in the plot ln $F_S(x)$ vs x^2, the slope of the curve may be interpreted as $-\alpha_s^2/5$ and the intercept as ln β_s. Therefore the Guinier radius will be $R_G(t) = \alpha_s k_s^{-1}(t)$ and $J_G(t) = \beta_s J_s(t)$ and the normalized scaling function F_G may be written as given by relation (4.6) $F_G(x) = \beta_s^{-1} F_s(\chi/\alpha_s)$.

5. GENERAL EXPRESSION FOR THE SCALING FUNCTION F_G

5.1. Computer simulations

The scaling function F_G has been determined for all points in the phase diagram indicated in Table 1. In Fig. 8 all these functions are plotted on a log–log scale. It appears that for large values of x all data points fall on the same smooth curve, represented by a thick line in Fig. 8. Hence for large values of x, the scaling function F_G is independent of the density ρ and the temperature T. This is not surprising in the x-region where the Guinier approximation, $F_G(x) = \exp(-x^2/5)$, is valid, but it is even true for much larger x. This corresponds to the idea explained in Section 3, that for large k the scattered intensity $S(k, t)$ is determined by the "single cluster function". We define this "single cluster function" $\Phi(x)$ as being equal to $\exp(-x^2/5)$ for small x (thin line in Fig. 8) and to $F_G(x)$ for large x (thick line in

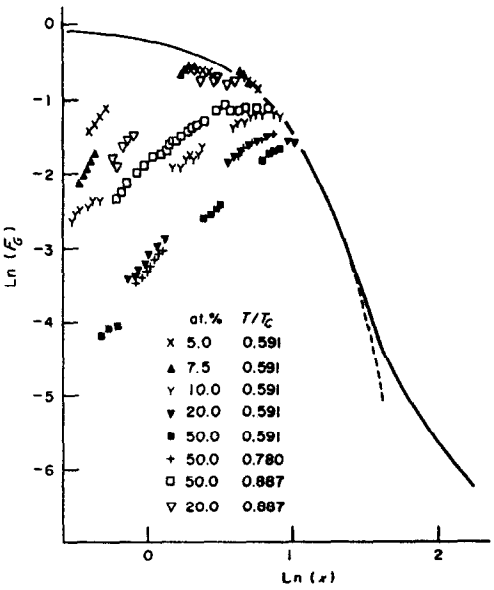

Fig. 8. Plot of ln $[F_G(x)]$ against ln x for the points 1–8 in the Ising model phase diagram (see Table 1). The thick line symbolises a high density of data points due to the superposition of all the curves. The thin line (full at one end, broken at the other) corresponds to the Guinier approximation $F_G(x) = \exp(-x^2/5)$. The "single cluster function" Φ is then defined as the thick full line extrapolated by the thin full line.

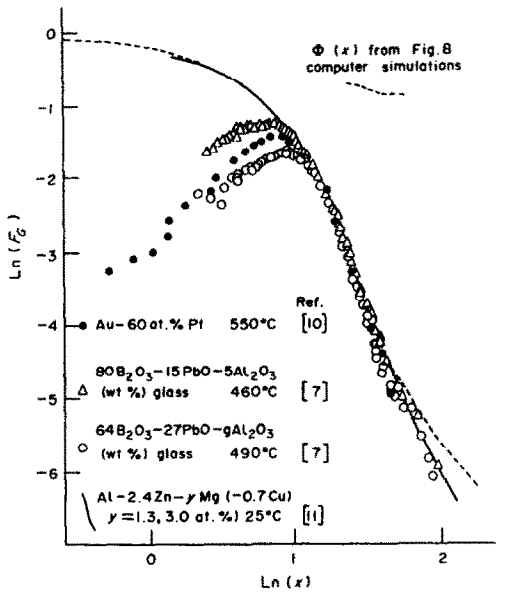

Fig. 9. Plot of ln $[F_G(x)]$ against ln x for several real systems. Broken line is the function Φ as taken from Fig. 8 (computer simulations), full line are data from Ref. [11] and the other symbols are data from Refs [7] and [10].

Fig. 8). Therefore using equations (3.4) and (4.4) we write

$$F_G(x) = \Phi(x) \cdot H[x/R_G(t), t]. \tag{5.1}$$

It follows that $H[x/R_G(t), t] = H_1(x)$ is independent of time and equal to 1 for large x [i.e. when $\Phi(x) = F_G(x)$]. H_1 is density and temperature dependent, whereas $\Phi(x)$ is a universal function independent of ρ and T (see Fig. 8), at least for these computer simulations.

5.2. *Real systems*

(a) Au–60 at.% Pt: decomposition in this sytem at $T = 550°C$ $(T/T_c = 0.6)$ has been studied by neutron scattering [10]. The scaling function of Ref. [15] has been normalized to give F_G as indicated in Section 4.2. and is shown in Fig. 9.

(b) B_2O_3–PbO–Al_2O_3 glass: recently the scaling hypothesis has been tested in this sytem using k_m as scaling length [7]. Scaling behaviour was confirmed but discrepancies for some of the curves were observed. Nevertheless these discrepancies are probably due, as pointed out by the authors, to the intrinsic inaccuracy in determining the position k_m of the intensity maxima. Figure 9 shows that the curves fit together perfectly when the "natural scaling" method described in Section 4.2 is used.

(c) Al–Zn–Mg–(Cu): neutron scattering data for these ternary (quaternary) alloys were reanalyzed and Fig. 9 shows that the structure functions scale very well [11].

For all these systems the normalised scaling functions F_G were plotted on a log–log scale in Fig. 9, together with the "single cluster function" Φ taken from the computer simulations (Fig. 8). It appears that the experimental data agree perfectly with each other for large values of x. Therefore the true scaling function $F_G(x)$ is, for large x, independent of density, temperature and even the substance investigated, which can be binary, ternary of even amorphous. This seems to conform the existence of a universal function $\Phi(x)$ (the single cluster function), describing the structure function at large values of k.

There is a small discrepancy between the computer data and real systems at very large x (Fig. 9). If we take as the correct shape for ϕ the one determined by the real experiments, thus $\phi(x) \sim 7/x^4$ for large x. This x^{-4} dependence is known as Porod law [16].

5.3. *The cluster interference function*

The existence of the universal function ϕ enables us to define both for real and for computer experiments the function

$$H_1(x) = F_G(x)/\Phi(x) \tag{5.2}$$

which should describe the effect of cluster interference. Here we can find an analogy to the language of molecular liquids, where the so called liquid structure factor $L(k)$ is obtained by dividing the total scattered intensity by the intensity scattered by a single molecule [25]. Since F_G is the scaled total intensity, we consider ϕ the scaled intensity of a single cluster, then H_1 is analogous to $L(k)$. In molecular liquids $L(k)$, small near $k = 0$, rises to a maximum at k_m and then has damped oscillations of period $\sim k_m$ [25]. In the case of solid solutions, which we are treating here, $H_1(x)$ also first grows with x but then quickly reaches the constant value 1.

H_1 has been plotted on a log–log scale in Fig. 10, including both real and computer experiments. By shifting these data along the x-axis by a certain amount, ln (δ) (a function of the substance, its composition, and the annealing temperature) a fairly good superposition of the data may be obtained for ranges of. This suggests that one writes

$$H_1(x) = \psi(\delta x). \tag{5.3}$$

The values of δ used to get the superposition are listed in Table 2. It appears that δ is smaller for experiments deep inside the miscibility gap. However the idea that δ is related to some mean distance between clusters was not confirmed accurately in the computer simulation: the expected proportionality $\delta \sim \rho^{-1/3}$ was not confirmed.

For the samples where $\delta < 0.38$ the "cluster interference function" ψ may be represented fairly well by $\psi(x) = x^3$ for $x < 1$; and $\psi = 1$ otherwise. When $\delta > 0.38$ a better approximation is $\psi(x) = x^2$ for $x < 1$; and $\psi(x) = 1$ otherwise (see Fig. 10). This difference in ψ between "deep" and "shallow" quenches is not very well understood. Perhaps there is some relationship with the old spinodal dichotomy between the nucleation and growth regions inside the miscibility gap [12–14].

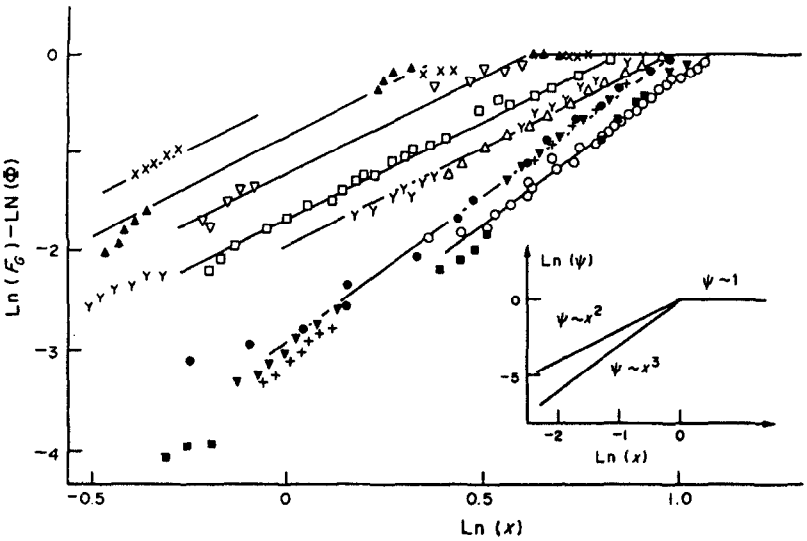

Fig. 10. The scaling functions F_G of Figs 8 and 9 have been divided by the "single cluster function" $\Phi(x)$ and put together in this log–log plot. The thick line, as in Fig. 8, is a superposition of many data points. The thin lines (with slopes 2 or 3) seem to fit the data for a given experiment (the symbols used are defined in Figs 8 and 9). Thereofre by shifting the data along the x-axis a superposition resulting in the function ψ drawn in the inset seems possible.

Nevertheless one should be careful interpreting the structure function for very small k in the case of computer experiments. There the smallest possible value of k is $2\pi/L$ and finite size effects are expected in this k-region. For instance, a single very long run at $T = 0.59T_c$ and $\rho = 50\%$ was undertaken, and after a very long time the maximum of the structure function could no longer shift to smaller k because of finite size effects distorting the scaling function. For the earlier times however there was no indication that size effects were important at these relatively shorter times.

Using the universal function ϕ and ψ, the final expression for the scaling function $F_G(x)$ is then given by (1.1). The corresponding form for the scattered intensity is

$$S(k, t) = J_G(t) \cdot \phi[k \cdot R_G(t)] \cdot \psi[k \cdot R_G(t) \cdot \delta(\rho, T)]. \quad (5.4)$$

This empirical relation recalls the expressions for the scattered intensity in the classical two phase models [16, 23] even if the "single cluster function" ϕ and the "cluster interference function" ψ are now somewhat different.

6. DISCUSSION

Structure functions of quenched binary alloys obtained from computer simulations performed at different quenching points in the coexistence regions were analysed to see how one may best get reliable data on the cluster size and density from the structure function. In all cases the first moment k_1, the position of the maximum k_{max} and the Guinier radius R_G were determined and, where it was possible (no percolation), cluster sizes and densities were also determined directly. During the scaling regime of the structure function, R_G, k_1^{-1} and k_{max}^{-1} are all proportional and consistent with the cluster sizes determined directly. Furthermore the Guinier radius gives a good description of the clusters even before the scaling regime and even in cases where the approximations in the Guinier model are not valid.

At early times however the agreement is very sensitive to the cutoffs chosen to compute the mean cluster size and density (Section 2.2) and also the background subtracted from the structure function (Section 2.3). Furthermore at all times, even during the scaling regime R_G, k_1^{-1} and k_{max}^{-1} are known only with low accuracy because they do not use all the information contained in $S(k, t)$. In order to get the best possible statistics, a graphical method, using the whole curve $S(k, t)$ vs k was developed for determining the scaled structure function. This should help in determining cluster sizes and numbers from $S(k, t)$.

When the so obtained scaling function is normalized to F_G, the structure function scaled with the Guinier radius R_G, it appears that the structure function for the computer simulations as well as for some real systems may be written as

$$S(k, t) = J_G(t) \cdot \phi[k \cdot R_G(t)] \cdot \psi[k \cdot R_G(t) \cdot \delta(\rho, t)]. \quad (5.4)$$

In analogy to classical two phase models [16] and molecular liquids [25] ψ is called the "cluster interference function" and ϕ the "single cluster function". δ seems to depend on how deep inside the miscibility gap the experiment is performed. At low

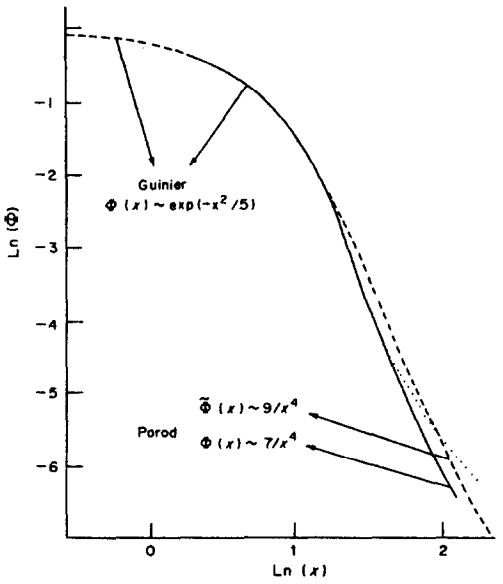

Fig. 11. The single cluster function $\Phi(x)$ has been represented in a log–log plot. Full line is due to experimental data (Fig. 9) and dots indicate a small deviation of the computer data from real systems at high values of x. A universal scaling function for the motion of random interfaces $\hat{I}(z)$ proposed recently by Ohta *et al.* [21] has been normalized to Guinier behaviour at small k by $\tilde{\Phi}(x) = \hat{I}(x \cdot \sqrt{3/5})/\hat{I}(0)$ and $\tilde{\Phi}$ is drawn with broken line. Besides the Guinier behaviour at small x, Φ and $\tilde{\Phi}$ have a λ/x^4 decay at high x (Porod law [16]). The value of λ for Φ and $\tilde{\Phi}$ is however somewhat different.

values of k, ψ describes the cluster interference, but at higher $k, \psi' = 1$ and $S(k, t)$ is determined uniquely by the Guinier radius $R_G(t)$ and the corresponding parameter $J_G(t)$. The universal function (x) is independent of density, temperature, and even of the substance investigated.

Recently Ohta *et al.* [21] have computed a universal scaling function for the motion of random interfaces. This function has like ϕ a Gaussian shape at small x and an x^{-4} behaviour at large x. To compare the function proposed by Ohta *et al.* [21] to $\phi(x)$ we have normalized the function $\hat{I}(z)$ from Ref. [26] so that it has the Guinier behaviour at small k. That is we define $\tilde{\phi}(x) = \hat{I}(x\sqrt{3/5})\hat{I}(0)$. This function $\tilde{\phi}(x)$ has been plotted in Fig. 11 (broken line) together with $\phi(x)$ determined by experiments on real systems (full line) and computer experiments (dots). There is a very good agreement in the region of Guinier behaviour ($x < 10$) but in the region of the $1/x^4$ decay (Porod law [16]) the function proposed by Ohta *et al.* provides values which are somewhat too high.

From this analysis it may be concluded that, during the scaling regime, the structure function follows, in the case of computer experiments as well as some real systems, a universal behaviour. Besides some effects at very small k (cluster interference) $S(k, t)$ is mainly determined by $V_G(t) = 4/3\ \pi\ R_G^3$, the mean cluster volume, and by $J_G(t)/V_G(t)$, the total number of clustered atoms. In fact when the structure function is scaled with $R_G(t)$ and $J_G(t)$, a universal curve is obtained, the main features of which may be understood in terms of Guinier and Porod laws. Nevertheless to get a quantitative understanding additional theoretical and experimental work has to be done.

Acknowledgements—This work was supported in part by NSF Grant DMR81-14726 and DOE Contract DE-AC02-76ER03077. P.F. was also supported in part by Fonds zur Förderung der Wissenschaftlichen Forschung in Österreich. He would like to thank O. Blaschko and G. Ernst for valuable discussions, and Professor Weinzierl for his continuous support. We all benefitted greatly from discussions with O. Penrose.

REFERENCES

1. G. Laslaz and P. Guyot, *Acta metall.* **25**, 277 (1977); R. J. Rioja and D. E. Laughlin, *Acta metall.* **28**, 1301 (1980).
2. T. Abe, K. Miyazaki and K.-I. Hirano, *Acta metall.* **30**, 357 (1982).
3. J. Merlin and G. Vigier, *Physica status Solidi* (a) **58**, 571 (1980).
4. A. Zahra, C. Y. Zahra, M. Laffitte, W. Lacom and H. P. Degischer, *Z. Metallk.* 70, 172 (1979).
5. A. Fontaine, P. Lagarde, A. Naudon, D. Raoux and D. Spanjaard, *Phil. Mag.* **B40**, 17 (1979); J. Mimault, A. Fontaine, P. Lagarde, D. Raoux, A. Sadoc and D. Spanjaard, *J. Phys. F, Metal Phys.* **11**, 1311 (1981).
6. K. B. Rundman and J. E. Hilliard, *Acta metall.* **15**, 1025 (1967); A. F. Bonfiglioli and A. Guinier, *Acta metall.* **14**, 1213 (1966); X. Auvray, P. Georgopoulos and J. B. Cohen, *Acta metall.* **29**, 1061 (1981).
7. A. Craievich and J. M. Sanchez, *Phys. Rev. Lett.* **47**, 1308 (1981; S. Bras, A. Craievich, J. M. Sanchez, C. Williams and E. D. Zanotto, preprint.
8. Y. C. Chou and W. I. Goldburg, *Phys. Rev.* **A20**, 2105 (1979); **A23**, 858 (1981).
9. G. Laslaz, P. Guyot and G. Kostorz, *J. Phys. Paris* **C7**, 406 (1977); M. Hennion, D. Ronzaud and P. Guyot, *Acta metall.* **30**, 599 (1982).
10. S. P. Singhal and H. Herman, *J. appl. Crystallogr.* **11**, 572 (1978).
11. O. Blaschko, G. Ernst, P. Fratzl, M. Bernole and P. Auger, *Acta metall.* **30**, 547 (1982).
12. J. W. Cahn, *Trans. Metall. Soc. A.I.M.E.* **242**, 166 (1968).
13. H. E. Cook, *Acta metall.* **18**, 297 (1970).
14. J. S. Langer, *Acta metall.* **21**, 1649 (1973); J. S. Langer, M. Bar-on and H. D. Miller, *Phys. Rev.* **A11**, 1417 (1975).
15. A. B. Bortz, M. H. Kalos, J. L. Lebowitz and M. A. Zendejas, *Phys. Rev.* **B10**, 535 (1974); J. Marro, A. B. Bortz, M. H. Kalos and J. L. Lebowitz, *Phys. Rev.* **B12**, 2000 (1975); A. Sur, J. L. Lebowitz, J. Marro and M. H. Kalos, *Phys. Rev.* **B15**, 3014 (1977); M. Rao, M. H. Kalos, J. L. Lebowtiz and J. Marro, *Phys. Rev.* **B13**, 4328 (1976); K. Binder, M. Kalos, J. Lebowitz and J. Marro, *Adv. Coll. Interface Sci.* **10**, 173 (1979); J. Marro, J. Lebowitz and M. Kalos, *Phys. Rev. Lett.* **43**, 282 (1979); J. L. Lebowitz, J. Marro and M. H. Kalos, *Acta metall.* **30**, 297 (1988).
16. A. Guinier and G. Fournet, *Small Angle Scattering of X-Rays* Wiley, New York (1955).
17. I. M. Lifshitz and V. V. Slyozov, *J. Phys. Chem. Solids* **19**, 35 (1961).
18. K. Binder and D. Stauffer, *Phys. Rev. Lett.* **33**, 1006 (1974); *Ad. Phys.* **25**, 343 (1976); P. Mirold and K. Binder, *Acta metall.* **25**, 1435 (1977); K. Binder, C. Billotet and P. Mirold, *Z. Phys.* **B30**, 183 (1978).
19. H. Furukawa, *Prog. Theor. Phys.* **59**, 1072 (1978); *Phys. Rev. Lett.* **43**, 136 (1979); *Phys. Rev.* **A23**, 1535 (1981).
20. P. A. Rikvold and J. D. Gunton, *Phys. Rev. Lett.* **49**, 286 (1982).
21. T. Ohta, D. Jasnow and K. Kawasaki, *Phys. Rev. Lett.* **49**, 1223 (1982).

22. K. Kawasaki, in *Phase Transitions and Critical Phenomena* (edited by C. Domb and M. S. Green), Vol. 2. Academic Press, New York (1972).
23. J. W. Essam and M. Fisher, *J. chem. Phys.* **38**, 802 (1963).
24. D. de Fontaine, *Solid St. Phys.* **34**, 73 (1979).
25. P. W. Schmidt and C. W. Tompson, in *Simple Dense Fluids* (edited by H. L. Frisch and Z. W. Salsburg), p. 31. Academic Press, New York (1968).